

1
2
3
4
5
6
7
8
9
10
11
12
13
14
15
16
17
18
19
20
21
22
23
24
25
26
27
28
29
30
31
32
33
34
35
36
37
38
39
40
41
42
43
44
45
46
47
48
49
50
51
52
53
54
55
56

Low temperature X-ray absorption spectroscopy study of CuMoO₄ and CuMo_{0.90}W_{0.10}O₄ using reverse Monte-Carlo method

Inga Jonane^{a,*}, Arturs Cintins^a, Aleksandr Kalinko^b, Roman Chernikov^c, Alexei Kuzmin^a

^a*Institute of Solid State Physics, University of Latvia, Kengaraga street 8, LV-1063 Riga, Latvia*

^b*Universität Paderborn, Naturwissenschaftliche Fakultät, Department Chemie, Warburger Strasse 100, 33098 Paderborn, Germany*

^c*DESY Photon Science, Notkestraße 85, D-22607 Hamburg, Germany*

Abstract

Reversible thermochromic phase transition between α - and γ -phases was studied in CuMoO₄ and CuMo_{0.90}W_{0.10}O₄ using X-ray absorption spectroscopy in the temperature range of 10–300 K. Reverse Monte Carlo modelling with evolutionary algorithm approach at several absorption edges simultaneously was applied to extract structural information encoded in the experimental EXAFS spectra. The obtained results show that an addition of 10 mol% of tungsten to CuMoO₄ induces local distortions in the structure and stabilizes the γ -phase, leading to an increase of the phase transition temperature by ~50-100 K.

Keywords: CuMoO₄, X-ray absorption spectroscopy, EXAFS, XANES, reverse Monte Carlo

*Corresponding author
E-mail address: inga.jonane@cfi.lu.lv (Inga Jonane).

57
58
59
60
61
62
63
64
65
66
67
68
69
70
71
72
73
74
75
76
77
78
79
80
81
82
83
84
85
86
87
88
89
90
91
92
93
94
95
96
97
98
99
100
101
102
103
104
105
106
107
108
109
110
111
112

1. Introduction

Copper molybdate (CuMoO₄) exhibits thermochromism and piezochromism ([Wiesmann et al. \(1997\)](#)) originated from the first-order structural phase transition accompanied with a drastic colour change between green and brownish-red. While both phases have triclinic $P\bar{1}$ symmetry, the crystal structure of γ -CuMoO₄ is built up of distorted CuO₆ and MoO₆ octahedra, whereas the structure of α -CuMoO₄ is composed of distorted CuO₆ octahedra, CuO₅ square-pyramids and MoO₄ tetrahedra. According to the pressure-temperature phase diagram ([Wiesmann et al. \(1997\)](#)), α -to- γ phase transition takes place during cooling below \sim 200 K or at room temperature (RT) by applying \sim 0.2 GPa pressure. Furthermore, the phase transition temperature can be increased by inducing chemical pressure upon substitution of molybdenum ions with tungsten ones ([Gaudon et al. \(2007a\)](#)). Depending on the tungsten concentration in CuMo_{1-x}W_xO₄ solid solutions, phases isostructural to high pressure CuMoO₄ can be obtained ([Wiesmann et al. \(1997\)](#); [Yanase et al. \(2013\)](#); [Benchikhi et al. \(2017\)](#)).

The most attractive for technological applications compound in the solid solution series is CuMo_{0.90}W_{0.10}O₄, because of its ability to switch between the two allotropic forms (α and γ) in the temperature range from 0 to 100 °C ([Gaudon et al. \(2007a\)](#); [Yanase et al. \(2013\)](#); [Robertson et al. \(2015\)](#); [Blanco-Gutierrez et al. \(2015\)](#)). It was shown ([Gaudon et al. \(2007b\)](#)) that a pressure induced by a finger is enough to promote α -to- γ phase transition in CuMo_{0.90}W_{0.10}O₄ at RT. The compound exhibits also halochromic properties, i.e. colour change upon solution pH variation, induced by surface protonation ([Gaudon et al. \(2010\)](#)). A pronounced thermosalient ("jumping crystals") effect caused by the phase transition has been also observed in CuMo_{0.90}W_{0.10}O₄ ([Robertson et al. \(2015\)](#)).

In order to better understand the structure-property relationships in CuMo_{1-x}W_xO₄, we performed temperature-dependent X-ray absorption spectroscopy (XAS) studies. We have shown recently ([Jonane et al. \(2018c\)](#)) that a variation of the X-ray absorption near edge structure (XANES) at the Mo K-edge in CuMoO₄ correlates with a degree of the molybdenum–oxygen coordination polyhedra distortion, both showing the hysteretic behavior upon α -to- γ phase transition (Fig. 1).

113
114
115
116
117
118
119

Extended X-ray absorption fine structure (EXAFS) data analysis of CuMoO₄ and CuMo_{0.90}W_{0.10}O₄ is challenging task due to the low symmetry of the α and γ phases, leading to a distortion of the local environment. In such case, the conventional EXAFS analysis is less effective because of a large number of fitting parameters required. Previously, we have employed a regularization-like method to reconstruct the radial distribution functions (RDFs) within the first coordination shell of Mo atoms in CuMoO₄ (Jonane et al. (2018b)). Here we extend our analysis beyond the first shell using advanced reverse Monte-Carlo (RMC) calculations based on evolutionary algorithm (Timoshenko et al. (2014c)) at several absorption edges simultaneously. We compare pure CuMoO₄ and CuMo_{0.90}W_{0.10}O₄ with the aim to understand the role of tungsten in the functional properties of CuMo_{1-x}W_xO₄ solid solutions.

134
135

2. Experimental

136
137
138
139
140
141
142
143
144

Polycrystalline CuMoO₄ powder was synthesized using solid-state reaction method by heating a mixture of CuO and MoO₃ powders at 650 °C in air for 8 hours followed by cooling down naturally to room temperature. The same synthesis method was applied for CuMo_{0.90}W_{0.10}O₄ by adding stoichiometric amount of WO₃. The as-prepared green powders had α -phase, confirmed by X-ray diffraction.

145
146
147
148
149
150
151
152
153
154
155
156
157
158
159
160
161

Temperature-dependent XAS experiments were conducted at the HASYLAB/DESY PETRA-III P65 undulator beamline. The storage ring was operated at $E=6.08$ GeV and current $I=95$ mA in top-up 40 bunch mode. The X-ray absorption spectra were collected at the Cu (8979 eV) and Mo (20000 eV) K-edges and W (10207 eV) L₃-edge during heating and cooling in transmission mode using two ionization chambers. Fixed exit Si(311) double-crystal monochromator was used in experimental set-up, and harmonic rejection was achieved by a coated silicon plane mirror. The Oxford Instruments liquid helium flow cryostat was used to maintain the sample temperature in the range of 10-300 K. The powder samples for XAS measurements were deposited on Millipore filters. The XAS experiment was performed starting at 300 K, next cooling down to 10 K, following by heating up to 300 K, again cooling down to 50 K and finally heating back to 300 K (Fig. 2).

162
163
164
165
166
167
168

169
170
171
172
173
174
175
176
177
178
179
180
181
182
183
184
185
186
187
188
189
190
191
192
193
194
195
196
197
198
199
200
201
202
203
204
205
206
207
208
209
210
211
212
213
214
215
216
217
218
219
220
221
222
223
224

3. Reverse Monte Carlo calculations

The experimental EXAFS spectra were analysed using the RMC method based on evolutionary algorithm (EA), as implemented in the EvAX code ([Timoshenko et al. \(2014c\)](#)). The details of the RMC method were reported by us previously and can be found in ([Timoshenko et al. \(2012\)](#)). The method was successfully used for interpretation of EXAFS spectra of numerous materials ([Timoshenko et al. \(2014a,b\)](#); [Kalinko et al. \(2016\)](#); [Jonane et al. \(2016\)](#); [Timoshenko et al. \(2017\)](#); [Jonane et al. \(2018a\)](#)).

Starting structure models of CuMoO₄ corresponding to the α and γ phases were constructed based on the diffraction data ([Wiesmann et al. \(1997\)](#)). The model for CuMo_{0.90}W_{0.10}O₄ was created by randomly substituting Mo atoms with W atoms in α -CuMoO₄ and γ -CuMoO₄ structures keeping the stoichiometric ratio of the elements. Several random substitutions were tested. Note that in our RMC method all coordination numbers correspond to that from the diffraction since average crystallographic structure is the starting point of the RMC procedure, and only small displacements of atoms, simulating thermal vibrations, are allowed during the RMC fit.

The RMC calculations were performed using periodic boundary conditions for $4a_0 \times 4b_0 \times 4c_0$ (a_0 , b_0 and c_0 are the lattice parameters) large supercell, containing 2304 atoms. All atoms in the supercell were randomly displaced at each RMC iteration with the maximum allowed displacement of 0.4 Å. The configuration-averaged EXAFS spectra at the Cu and Mo K-edges and additionally at the W L₃-edge for CuMo_{0.90}W_{0.10}O₄ were calculated using the ab initio self-consistent real-space multiple-scattering (MS) FEFF8.5L code ([Ankudinov et al. \(1998\)](#)) taking into account MS contributions up to the 6th order. The complex energy-dependent exchange-correlation Hedin-Lundqvist potential ([Hedin and Lundqvist \(1971\)](#)) was employed to account for inelastic effects. The amplitude scaling parameter $S_0^2 = 1$ was used in all simulations. Comparison between the experimental and theoretical EXAFS spectra was performed in direct (R) and reciprocal (k) space simultaneously using the Morlet wavelet transform ([Timoshenko and Kuzmin \(2009\)](#)). The convergence of RMC simulations was achieved after several thousand of iterations.

The RMC calculations of the experimental data close to γ -to- α phase transition

225
226
227
228
229
230
231
232
233
234
235
236
237
238
239
240
241
242
243
244
245
246
247
248
249
250
251
252
253
254
255
256
257
258
259
260
261
262
263
264
265
266
267
268
269
270
271
272
273
274
275
276
277
278
279
280

temperature were performed using the structure models for both phases. The obtained fits for CuMoO₄ and CuMo_{0.90}W_{0.10}O₄ at selected temperatures are shown in Fig. 3 and 4, respectively. The final atomic configurations were used to calculate the partial RDFs $g(R)$ for further analysis.

4. Results and discussion

The linear combination analysis (LCA) of the Mo K-edge XANES performed in the temperature range from 10 to 300 K, as described in [Jonane et al. \(2018c\)](#), indicates that the phase transition hysteresis in CuMo_{0.90}W_{0.10}O₄ is shifted to higher temperatures (Fig. 1) in agreement with previous studies ([Gaudon et al. \(2007a,b\)](#); [Yanase et al. \(2013\)](#)). The transition from α to γ phase occurred between 250 and 100 K upon cooling, whereas the transition from γ to α phase started at about 280 K upon heating and was still not finished at room temperature even several hours after. Optical, calorimetry and magnetic measurement experiments showed that the γ -to- α phase transition in CuMo_{0.90}W_{0.10}O₄ occurs during heating in the temperature range between 340 and 380 K ([Gaudon et al. \(2007a\)](#)).

Temperature-dependent EXAFS spectra of CuMoO₄ and CuMo_{0.90}W_{0.10}O₄ are shown in Fig. 2. One can see that the Cu K-edge spectra are weakly affected during heating from 10 K to 300 K, however some changes occur at 250 K and can be attributed to the transition from CuO₆ octahedra to CuO₅ square-pyramids. The Mo K-edge is drastically affected during the phase transition because molybdenum coordination changes from octahedral to tetrahedral. Finally, it seems that the local environment of tungsten atoms does not change significantly during the whole cooling and heating experiments.

More detailed analysis can be performed based on the results of RMC calculations reported in Fig. 3 for CuMoO₄ and in Fig. 4 for CuMo_{0.90}W_{0.10}O₄. Note that the RMC models agree well with the EXAFS spectra at two or three absorption edges, which is crucial for accurate reconstruction of crystal structure for multi-atom compounds ([Timoshenko et al. \(2014a\)](#)).

The experimental EXAFS spectra of CuMoO₄ at $T=200$ and 300 K (Fig. 3) are well described by the structure models of γ and α phases, respectively. At the same

281
282
283
284
285
286
287

time, the structure models of both α and γ phases give reasonable agreement with the experimental data at $T=250$ K, indicating coexistence of the two phases in close ratio. This conclusion agrees with the LCA results suggesting the presence of the 60% and 40% of γ and α phases, respectively ([Jonane et al. \(2018b\)](#)).

293 The results of RMC calculations using α and γ phase structures for CuMo_{0.90}W_{0.10}O₄
294 are shown in Fig. 4. At $T=50$ K, the EXAFS spectra at the Cu, Mo and W absorption
295 edges are well reproduced using the γ -phase structure model. At the same time, at
296 $T=300$ K (before cooling), the α -phase model gives good agreement at the Cu and Mo
297 K-edges, but slightly worse agreement at the W L₃-edge, indicating that some relax-
298 ation of the local environment around tungsten ions occurs. Indeed, the W L₃-edge EX-
299 AFS can be slightly better described by the γ -phase structure, which does not apply to
300 the other two edges. This means that in spite of the crystal lattice of CuMo_{0.90}W_{0.10}O₄
301 at $T=300$ K (before cooling) corresponds to that in the α -phase, the local structure
302 around W atoms relaxes in an attempt to reconstruct distorted octahedral coordination.
303

307 The partial RDFs for Cu–O, Mo–O and W–O atom pairs, calculated from the atom
308 coordinates of the RMC models of CuMoO₄ and CuMo_{0.90}W_{0.10}O₄, are compared in
309 Fig. 5. Note that the reported RDFs are averaged over all atoms of the same type within
310 the supercell. However, one can also distinguish three non-equivalent crystallographic
311 sites of Cu and Mo atoms with different local environment in CuMoO₄.
312

314 Further we will consider the nearest groups of oxygen atoms located around metal
315 ions at the distances up to about 3.5 Å. One can see that the Cu and Mo environments
316 are close in both CuMoO₄ and CuMo_{0.90}W_{0.10}O₄ compounds. At the same time, while
317 the Cu environment is quite similar also at low (50 K) and high (300 K) temperatures,
318 the distributions of the Mo–O atom pairs differ significantly already for the closest
319 4 oxygen atoms. The tetrahedral coordination in α -phase is more ordered than the
320 octahedral one in γ -phase. In fact, the MoO₆ octahedra are strongly distorted with a
321 distribution of the Mo–O distances from ~1.5 Å to ~2.8 Å. The group of four nearest
322 oxygen atoms is responsible for a sharp peak in the RDFs at ~1.8 Å. These results
323 are in agreement with those obtained by the regularization-like method ([Jonane et al.](#)
324 (2018b)).
325

326 Next, we compare the W–O and Mo–O distributions in CuMo_{0.90}W_{0.10}O₄ to un-
327

328
329
330
331
332
333
334
335
336

337
338
339
340
341
342

343 derstand how large is the local structure relaxation around tungsten atoms. At low
344 temperature (50 K) in γ -phase, tungsten atoms have distorted octahedral coordination
345 close to that of molybdenum (Fig. 5(E)). The distortion of WO₆ and MoO₆ octahedra
346 is due to the second-order Jahn–Teller effect ([Kunz and Brown \(1995\)](#)) caused by the
347 charge transfer from oxygen atoms surrounding metal ion, having formally 6+ oxidation
348 state (5d⁰ electron configuration). At T=300 K in α -phase, when the coordination
349 of molybdenum atoms becomes tetrahedral, tungsten atoms tend to have more distorted
350 environment (Fig. 5(F)): there is an additional group of oxygen atoms at about 2.1 Å,
351 and the next group of oxygen atoms at 2.8 Å is slightly displaced and split. Moreover,
352 the RMC calculations at the W L₃-edge for α -CuMo_{0.90}W_{0.10}O₄ using the structure
353 model corresponding to γ -phase (W in distorted octahedral environment) give slightly
354 better agreement with the experiment, however, the shape of the W–O distribution is
355 quite similar to that in the α -phase.
356

357 To conclude, our results confirm the tendency of tungsten atoms in CuMo_{0.90}W_{0.10}O₄
358 to adapt distorted octahedral environment when substituting molybdenum atoms, thus
359 affecting the temperature/pressure of α -to- γ phase transition and helping to stabilize
360 γ -phase at room temperature.
361

362
363
364
365
366
367
368 **5. Conclusions**
369

370 X-ray absorption spectroscopy was used to probe a variation of the local atomic
371 structure in CuMoO₄ and CuMo_{0.90}W_{0.10}O₄ in the temperature range of 10–300 K.
372 Advanced data analysis of EXAFS spectra at several absorption edges simultaneously
373 interpreted by reverse Monte Carlo method allowed us to monitor the α -to- γ and γ -to- α
374 thermochromic phase transitions, occurring gradually with the two phase coexistence
375 range. We observed that the addition of 10 mol% of tungsten to CuMoO₄ induces local
376 distortions and stabilizes the γ -phase, leading to an increase of the phase transition
377 temperature by ~50–100 K.
378
379
380
381
382
383
384
385
386
387
388
389
390
391
392

393
394
395
396
397
398
399**Acknowledgements**400
401
402
403
404
405
406

This work was supported by Scientific Research Project for Students and Young Researchers Nr. SJZ/2017/5 realized at the Institute of Solid State Physics, University of Latvia. The experiment at HASYLAB/DESY was performed within the project I-20160149 EC.

407
408**References**409
410

Ankudinov, A.L., Ravel, B., Rehr, J.J., Conradson, S.D., 1998. Real-space multiple-scattering calculation and interpretation of X-ray-absorption near-edge structure. Phys. Rev. B 58, 7565–7576. doi:[10.1103/PhysRevB.58.7565](https://doi.org/10.1103/PhysRevB.58.7565).

411
412
413
414

Benchikhi, M., El Ouatib, R., Guillemet-Fritsch, S., Er-Rakho, L., Durand, B., 2017. Investigation of structural transition in molybdates CuMo_{1-x}W_xO₄ prepared by polymeric precursor method. Process. Appl. Ceram. 11, 21–26. doi:[10.2298/PAC1701021B](https://doi.org/10.2298/PAC1701021B).

415
416
417
418
419
420
421

Blanco-Gutierrez, V., Cornu, L., Demourgues, A., Gaudon, M., 2015. CoMoO₄/CuMo_{0.9}W_{0.1}O₄ mixture as an efficient piezochromic sensor to detect temperature/pressure shock parameters. ACS Appl. Mater. Interfaces. 7, 7112–7117. doi:[10.1021/am508652h](https://doi.org/10.1021/am508652h).

422
423
424
425
426
427

Gaudon, M., Carbonera, C., Thiry, A.E., Demourgues, A., Deniard, P., Payen, C., Létard, J.F., Jobic, S., 2007a. Adaptable thermochromism in the CuMo_{1-x}W_xO₄ series ($0 \leq x < 0.1$): A behavior related to a first-order phase transition with a transition temperature depending on x . Inorg. Chem. 46, 10200–10207. doi:[10.1021/ic701263c](https://doi.org/10.1021/ic701263c).

428
429
430
431
432
433
434

Gaudon, M., Deniard, P., Demourgues, A., Thiry, A.E., Carbonera, C., Le Nestour, A., Largeau, A., Létard, J.F., Jobic, S., 2007b. Unprecedented "one-finger-push"-induced phase transition with a drastic color change in an inorganic material. Adv. Mater. 19, 3517–3519. doi:[10.1002/adma.200700905](https://doi.org/10.1002/adma.200700905).

435
436
437
438
439
440
441
442443
444
445
446
447
448

449
450
451
452
453
454
455
456
457
458
459
460
461
462
463
464
465
466
467
468
469
470
471
472
473
474
475
476
477
478
479
480
481
482
483
484
485
486
487
488
489
490
491
492
493
494
495
496
497
498
499
500
501
502
503
504

- Gaudon, M., Riml, C., Turpaine, A., Labrugere, C., Delville, M.H., 2010. Investigation of the chromic phase transition of CuMo_{0.9}W_{0.1}O₄ induced by surface protonation. Chem. Mater. 22, 5905–5911. doi:[10.1021/cm101824d](https://doi.org/10.1021/cm101824d).
- Hedin, L., Lundqvist, B.I., 1971. Explicit local exchange-correlation potentials. J. Phys. C: Solid State Phys. 4, 2064–2083. doi:[10.1088/0022-3719/4/14/022](https://doi.org/10.1088/0022-3719/4/14/022).
- Jonane, I., Anspoks, A., Kuzmin, A., 2018a. Advanced approach to the local structure reconstruction and theory validation on the example of the W L₃-edge extended X-ray absorption fine structure of tungsten. Modelling Simul. Mater. Sci. Eng. 26, 025004. doi:[10.1088/1361-651X/aa9bab](https://doi.org/10.1088/1361-651X/aa9bab).
- Jonane, I., Cintins, A., Kalinko, A., Chernikov, R., Kuzmin, A., 2018b. Probing the thermochromic phase transition in CuMoO₄ by EXAFS spectroscopy. Phys. Status Solidi B 255, 1800074. doi:[10.1002/pssb.201800074](https://doi.org/10.1002/pssb.201800074).
- Jonane, I., Cintins, A., Kalinko, A., Chernikov, R., Kuzmin, A., 2018c. X-ray absorption spectroscopy of thermochromic phase transition in CuMoO₄. Low Temp. Phys. 44, 434–437. doi:[10.1063/1.5034155](https://doi.org/10.1063/1.5034155).
- Jonane, I., Lazdins, K., Timoshenko, J., Kuzmin, A., Purans, J., Vladimirov, P., Gräning, T., Hoffmann, J., 2016. Temperature-dependent EXAFS study of the local structure and lattice dynamics in cubic Y₂O₃. J. Synchrotron Rad. 23, 510–518. doi:[10.1107/S1600577516001181](https://doi.org/10.1107/S1600577516001181).
- Kalinko, A., Bauer, M., Timoshenko, J., Kuzmin, A., 2016. Molecular dynamics and reverse Monte Carlo modeling of scheelite-type AWO₄ (A= Ca, Sr, Ba) W L₃-edge EXAFS spectra. Phys. Scr. 91, 114001. doi:[10.1088/0031-8949/91/11/114001](https://doi.org/10.1088/0031-8949/91/11/114001).
- Kunz, M., Brown, I., 1995. Out-of-center distortions around octahedrally coordinated d⁰ transition metals. J. Solid State Chem. 115, 395–406. doi:[10.1006/jssc.1995.1150](https://doi.org/10.1006/jssc.1995.1150).
- Robertson, L., Penin, N., Blanco-Gutierrez, V., Sheptyakov, D., Demourgues, A., Gaudon, M., 2015. CuMo_{0.9}W_{0.1}O₄ phase transition with thermochromic,

505
506
507
508
509
510
511
512
513
514
515
516
517
518
519
520
521
522
523
524
525
526
527
528
529
530
531
532
533
534
535
536
537
538
539
540
541
542
543
544
545
546
547
548
549
550
551
552
553
554
555
556
557
558
559
560

piezochromic, and thermosalient effects. J. Mater. Chem. C 3, 2918–2924. doi:[10.1039/C4TC02463J](https://doi.org/10.1039/C4TC02463J).

Timoshenko, J., Anspoks, A., Kalinko, A., Kuzmin, A., 2014a. Analysis of extended x-ray absorption fine structure data from copper tungstate by the reverse Monte Carlo method. Phys. Scr. 89, 044006. doi:[10.1088/0031-8949/89/04/044006](https://doi.org/10.1088/0031-8949/89/04/044006).

Timoshenko, J., Anspoks, A., Kalinko, A., Kuzmin, A., 2014b. Temperature dependence of the local structure and lattice dynamics of wurtzite-type ZnO. Acta Mater. 79, 194–202. doi:[10.1016/j.actamat.2014.07.029](https://doi.org/10.1016/j.actamat.2014.07.029).

Timoshenko, J., Anspoks, A., Kalinko, A., Kuzmin, A., 2017. Thermal disorder and correlation effects in anti-perovskite-type copper nitride. Acta Mater. 129, 61–71. doi:[10.1016/j.actamat.2017.02.074](https://doi.org/10.1016/j.actamat.2017.02.074).

Timoshenko, J., Kuzmin, A., 2009. Wavelet data analysis of EXAFS spectra. Comp. Phys. Commun. 180, 920–925. doi:[10.1016/j.cpc.2008.12.020](https://doi.org/10.1016/j.cpc.2008.12.020).

Timoshenko, J., Kuzmin, A., Purans, J., 2012. Reverse Monte Carlo modeling of thermal disorder in crystalline materials from EXAFS spectra. Comp. Phys. Commun. 183, 1237–1245. doi:[10.1016/j.cpc.2012.02.002](https://doi.org/10.1016/j.cpc.2012.02.002).

Timoshenko, J., Kuzmin, A., Purans, J., 2014c. EXAFS study of hydrogen intercalation into ReO₃ using the evolutionary algorithm. J. Phys.: Condens. Matter 26, 055401. doi:[10.1088/0953-8984/26/5/055401](https://doi.org/10.1088/0953-8984/26/5/055401).

Wiesmann, M., Ehrenberg, H., Miehe, G., Peun, T., Weitzel, H., Fuess, H., 1997. *p-T* phase diagram of CuMoO₄. J. Solid State Chem. 132, 88–97. doi:[10.1006/jssc.1997.7413](https://doi.org/10.1006/jssc.1997.7413).

Yanase, I., Mizuno, T., Kobayashi, H., 2013. Structural phase transition and thermochromic behavior of synthesized W-substituted CuMoO₄. Ceram. Int. 39, 2059–2064. doi:[10.1016/j.ceramint.2012.08.059](https://doi.org/10.1016/j.ceramint.2012.08.059).

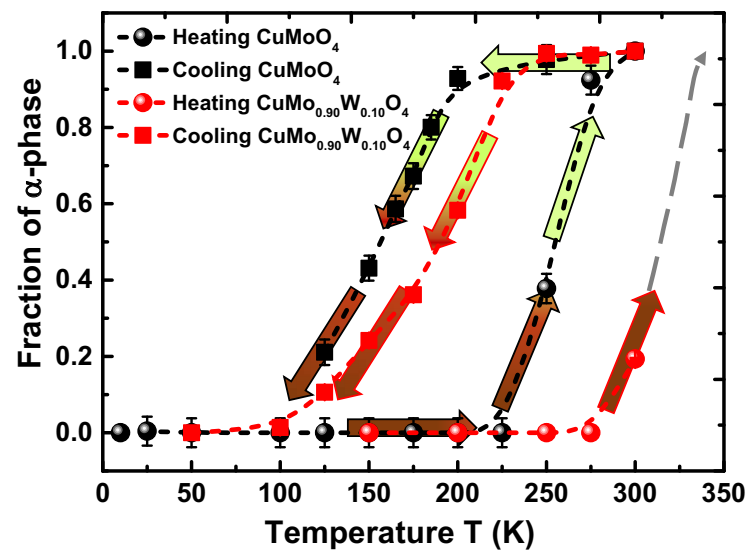
561
562
563
564
565
566
567
568
569
570
571
572
573
574
575
576
577
578
579
580
581
582
583
584
585
586
587
588
589
590
591
592
593
594
595
596
597
598
599
600
601
602
603
604
605
606
607
608
609
610
611
612
613
614
615
616

Figure 1: Temperature dependence of the fraction of α phase in CuMoO₄ and CuMo_{0.90}W_{0.10}O₄ samples upon heating and cooling. Gray dashed arrow is an extrapolation above the room temperature for CuMo_{0.90}W_{0.10}O₄.

617
 618
 619
 620
 621
 622
 623
 624
 625
 626
 627
 628
 629
 630
 631
 632
 633
 634
 635
 636
 637
 638
 639
 640
 641
 642
 643
 644
 645
 646
 647
 648
 649
 650
 651
 652
 653
 654
 655
 656
 657
 658
 659
 660
 661
 662
 663
 664
 665
 666
 667
 668
 669
 670
 671
 672

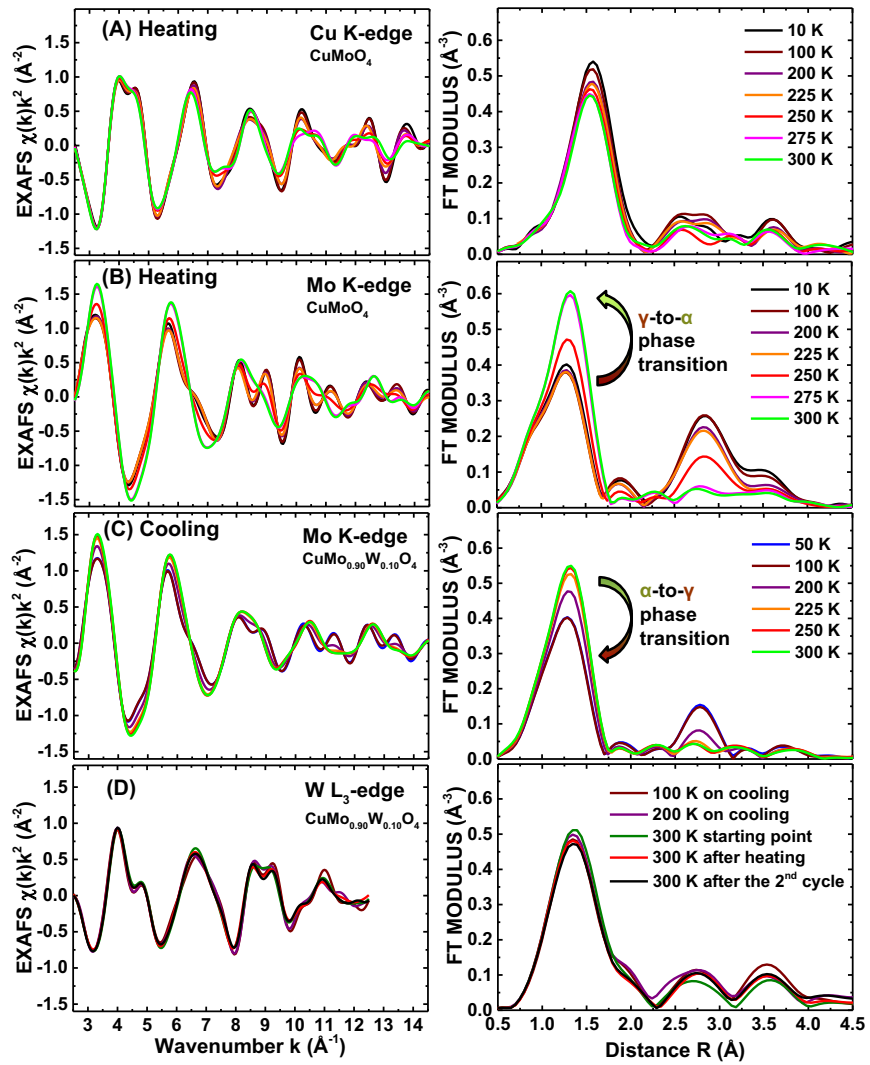


Figure 2: Temperature-dependence of the experimental EXAFS spectra $\chi(k)k^2$ and their Fourier transforms (FTs) for the Cu (A) and Mo (B) K-edges in CuMoO₄ during heating from 10 K to 300 K, for the Mo K-edge (C) in CuMo_{0.90}W_{0.10}O₄ during cooling from 300 K to 50 K and for the W L₃-edge (D) in CuMo_{0.90}W_{0.10}O₄ at different stages of the experiment.

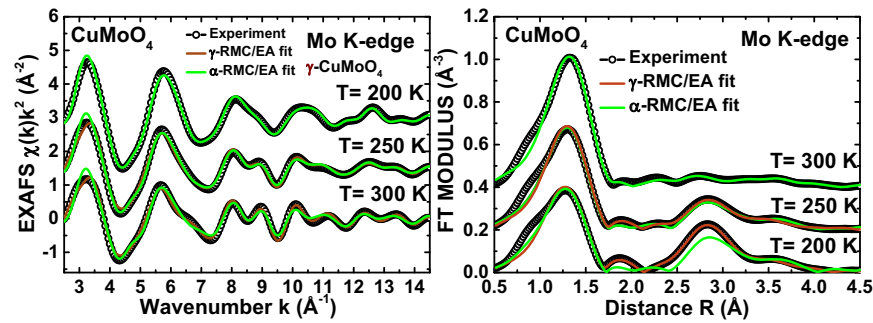
673
674
675
676
677
678
679
680681
682
683
684
685
686
687
688

Figure 3: Results of RMC calculations for the Mo K-edge in CuMoO₄ at selected temperatures. Left panel: the experimental and calculated EXAFS spectra $\chi(k)^2$ using α - and γ -CuMoO₄ initial structure models. Right panel: the corresponding Fourier transforms.

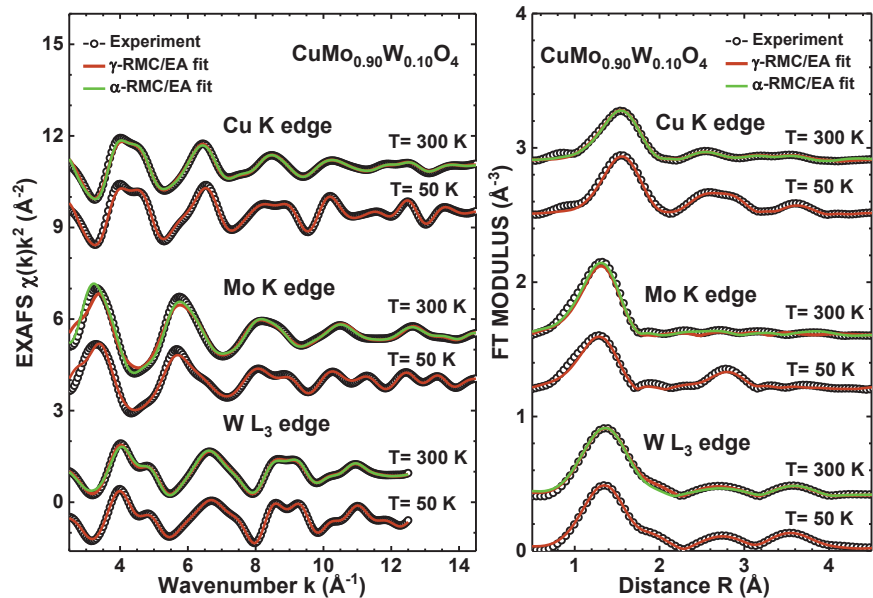
689
690
691692
693
694
695
696
697
698

Figure 4: Results of RMC calculations for the Cu K-edge, Mo K-edge and W L₃-edge in CuMo_{0.90}W_{0.10}O₄ at $T=50$ K (γ -phase) and $T=300$ K (α -phase). Left panel: the experimental and calculated EXAFS spectra $\chi(k)^2$. Right panel: the corresponding Fourier transforms.

717
718
719
720
721
722
723
724
725
726
727
728

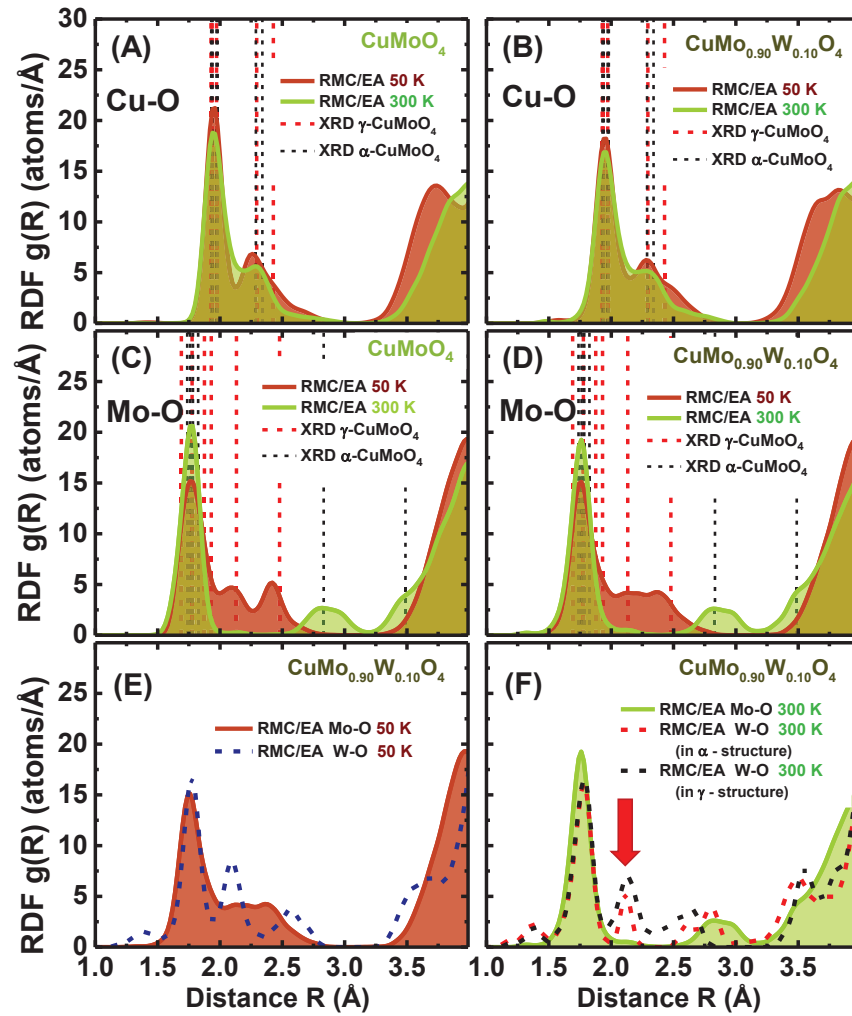
729
730
731
732
733
734
735
736
737
738
739
740
741
742
743
744
745
746
747
748
749
750
751
752
753
754
755
756
757
758
759
760
761
762
763
764
765
766
767
768
769

Figure 5: Radial distribution functions for Cu–O, Mo–O, W–O atom pairs in CuMoO₄ (A,C) and CuMo_{0.90}W_{0.10}O₄ (B,D,E,F), calculated from the atom coordinates of the RMC models. Dashed vertical lines show interatomic distances according to diffraction data (Wiesmann et al. (1997)). Vertical arrow in (F) indicates a group of oxygen atoms which does not exist in the tetrahedral coordination.

775
776
777
778
779
780
781
782
783
784

